

## **A Simple and Accurate Elastoplastic Model Dependent on the Third Invariant and Applied to a Wide Range of Stress Triaxiality**

**Lucival Malcher**

Department of Mechanical Engineering  
Faculty of Tecnology, University of Brasilia  
malcher@unb.br

**Edgar Nobuo Mamiya**

Department of Mechanical Engineering  
Faculty of Tecnology, University of Brasilia  
mamiya@unb.br

**Fabio Comes de Castro**

Department of Mechanical Engineering  
Faculty of Tecnology, University of Brasilia  
fabiocastro@unb.br

**João Vitor Sahadi Cavalheiro**

Automotive Engineering  
Faculty UnB at Gama, University of Brasilia  
Joao\_sahadi@aluno.unb.br

### **ABSTRACT**

In this contribution, a new and simple elastoplastic model is proposed and applied to a wide range of stress triaxiality. Regarding the constitutive formulation, a new equivalent stress is suggested depending now on the second and third invariant of the deviatoric stress tensor. The effect of the last one is introduced by the so-called normalized third invariant that is a ratio between the third invariant and the von Mises equivalent stress. The new proposition is then implemented in an academic finite element framework and through an operator split methodology the numerical model is determined. After that, numerical simulations are carried out regarding different load conditions. The numerical results obtained by the new proposition are compared with experimental data and classical elastoplastic models, such as: von Mises and Tresca. In the conclusions, it is shown that the new proposition is more accurate than the classical models for a wide range of stress triaxiality, regarding the level of displacement at fracture and the level of reaction force during the process.

**Keywords:** elastoplastic model, third invariant, stress triaxiality, ductile fracture

### **1 INTRODUCTION**

The theory based on the second invariant of the deviatoric stress tensor ( $J_2$ ), more widely known as the von Mises' model, is one of the most used formulations to describe the behavior of metals during the elasto-plastic regime. Such model (von Mises) assumes that the effect of the hydrostatic stress is negligible in the evolution of the plastic flow for ductile materials. The hydrostatic stress is a parameter responsible for controlling the size of the elastic regime (Bardet, 1990; Bai, 2008). Furthermore, in the von Mises' formulation, the effect of the third invariant of the deviatoric stress tensor (normally denoted by  $J_3$ ) is also ignored. The third invariant is a parameter

used in the definition of the Lode angle or Azimuth angle, which can be responsible for the shape of the yield surface (Bardet, 1990; Bai, 2008). Over the last five years, the importance of these two parameters in the description of the behavior of ductile materials, the hydrostatic stress and the Lode angle, has been clearly recognized and detailed studies were conducted by several authors (Bai *et al.*, 2007; Bai, 2008; Driemeier *et al.*, 2010; Mirone *et al.*, 2010; Gao *et al.*, 2011). Many researchers have done extensive experimental studies as Richmond & Spitzing (1980), who were the first researchers to study the pressure effects on the yielding of aluminium alloys. Later, Bardet (1990) proposed a methodology to describe the Lode angle dependence for some constitutive models, in addition Wilson (2002) conducted studies on notched 2024-T351 aluminium bars under tensile tests and verified the importance of these effects. Brunig *et al.* (1999) proposed a constitutive model with three invariants that could be applied to metal plasticity and fracture. According to Mirone *et al.* (2010), the phenomenon of ductile failure is influenced by the relation with the variables from the stress-strain characterization and the failure prediction is better described by the plastic strain, stress triaxiality and Lode angle parameters. An experimental program to study the influence of the stress tensor invariants in ductile failures was presented by Driemeier *et al.* (2010). This methodology can be seen as an efficient tool to investigate the effects of stress intensity, stress triaxiality and Lode angle. Recently, Gao *et al.* (2011) have proposed an elasto-plastic model, which is a function of the hydrostatic stress as well as the second and third invariants of the stress deviator. The initiation of the fracture is often preceded by large plastic deformation and there are considerable stress and strain gradients around the point of fracture. In such a case, the  $J_2$  theory is not accurate enough to capture the physical effects and more refined plasticity models have to be developed to be used in a larger range of loading conditions.

## 2 CONSTITUTIVE FORMULATION

Several factors have been systematically analysed in the study of ductile fracture, nevertheless, there are three factors that have gained increased interest: the hydrostatic stress ( $p$ ), stress triaxiality ( $\eta$ ), and the Lode angle ( $\theta$ ) expressed by *Equations* (1-3) respectively (Brunig *et al.*, 2008; Bai & Wierzbicki, 2008; Zadpoor *et al.*, 2009; Tvergaard, 2008; Nahshon *et al.*, 2008).

$$p = \frac{1}{3} \text{tr}(\boldsymbol{\sigma}), \quad (1)$$

$$\eta = -\frac{p}{q}, \quad (2)$$

$$\theta = \tan^{-1} \left\{ \frac{1}{\sqrt{3}} \left[ 2 \left( \frac{S_2 - S_3}{S_1 - S_3} \right) - 1 \right] \right\}, \quad (3)$$

where  $q = \sqrt{3/2 \mathbf{S}:\mathbf{S}}$  is the von Mises equivalent stress,  $\mathbf{S} = \boldsymbol{\sigma} - p\mathbf{I}$  is the deviatoric stress tensor and  $S_1$ ,  $S_2$  and  $S_3$  are the components of the deviatoric stress tensor in the principal plane. The Lode angle can also be written as a function of the so-called normalized third invariant of the deviatoric stress tensor, as presented below

$$\theta = \frac{1}{3} \arccos(\xi), \quad (4)$$

where  $\xi$  represents the normalized third invariant, that can be mathematically determined by a ratio between the third invariant and the von Mises equivalent stress

$$\xi = \left(\frac{r}{q}\right)^3 . \quad (5)$$

The term  $r$  represents the third invariant, alternatively, defined by Bai *et al.* (2007) and can be determined as following

$$r = \left[\frac{27}{2} J_3\right]^{1/3} = \left[\frac{27}{2} \det(\mathbf{S})\right]^{1/3} , \quad (6)$$

where  $J_3$  is the third invariant of the deviatoric stress tensor,  $\mathbf{S}$ . The Lode angle can also be normalized ( $\bar{\theta}$ ) and this parameter is known as the normalized Lode angle (Bai & Wierzbicki, 2008).

$$\bar{\theta} = 1 - \frac{6\theta}{\pi} . \quad (7)$$

The range of  $\bar{\theta}$  is  $-1 \leq \bar{\theta} \leq 1$ . According to many authors, the contribution of the effect of the third invariant is more severe than the contribution of the stress triaxiality effect in the plastic flow rule (see Bai *et al.*, 2008 and Gao, 2011). The definition of the Lode angle,  $\theta$ , can be better understood by analyzing the representation of the stress vector,  $\overline{OB}$ , on the principal stresses space as illustrated in *Figure 1(a)*.

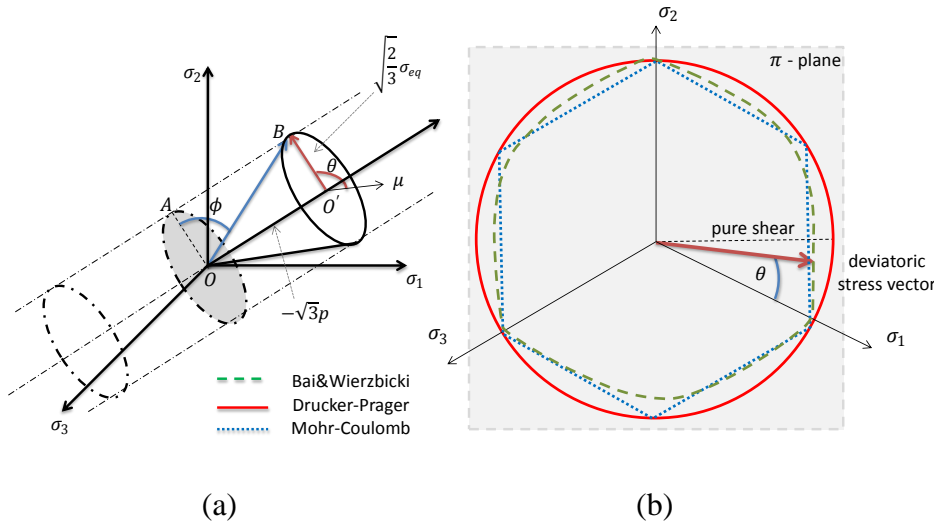


*Figure 1.* (a) Schematic representation of the stress vector  $\overline{OB}$  on the principal stresses space and (b) definition of the Lode angle on the  $\pi$ -plane. Adapted from Bai (2008).

The stress vector can be decomposed in two, a deviatoric  $\overline{OA}$  and a hydrostatic  $\overline{OO'}$  part. The ratio between the hydrostatic and deviatoric part is, by definition, the stress triaxiality which is associated with the angle  $\phi$ , that is the angle obtained between the stress vector  $\overline{OB}$  and the  $\pi$ -plane. Such angle, named elevator angle, is responsible for the size of the elastic regime. The Lode angle is defined on the  $\pi$ -plane or deviatoric plane, see *Figure 1b*, and is the smallest angle between the projection of the stress tensor on the deviatoric plane and the axis of the principal stresses. Bardet (1990) conducted several studies on the influence of the Lode angle on the shape of the yield

surface and concluded, for instance, that the Drucker-Prager model is Lode angle independent and Tresca and Mohr-Coulomb models are Lode angle dependent (*Figure 1b*).

In the context of ductile fracture, some researchers have suggested the introduction of the Lode angle effect either into the standard von Mises elasto-plastic constitutive model as into some damage evolution laws. In particular, Bao *et al.* (2004), Brünig *et al.* (2000) and Bai & Wierzbicki (2008) have proposed new elasto-plastic models that include the three invariants of the deviatoric stress tensor in the definition of the material yield surface. On the other hand, in order to improve the evolution of the porosity obtained by Gurson's theory for low level of stress triaxiality, Nahshon & Hutchinson (2008), Barsoum & Faleskog (2007) and Xue (2008) have proposed the introduction of new shear mechanisms in the damage evolution law of Gurson's model, which are Lode angle dependent. Within this framework, it is proposed a simple and accurate elastoplastic model wherein the equivalent stress is a combination between the von Mises equivalent stress and the normalized third invariant of the deviatoric stress tensor. Following the new proposition is described.

## 2.1 Yield stress in shear and tensile loading conditions

According to experimental evidences (see Wilson, 2002), it can be observed a difference between the yield stress of a material subjected to tensile and shear loading conditions. *Figure 2* illustrates the projection of the stress vector onto the  $\pi$ -plane.

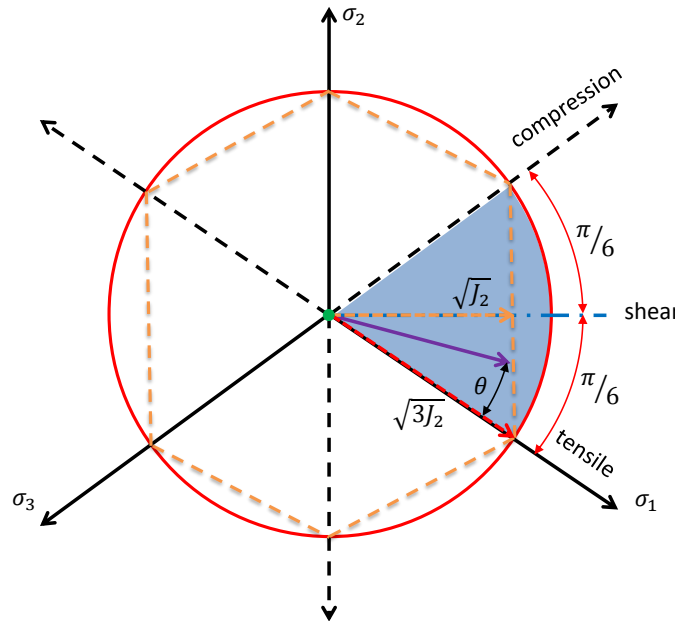


*Figure 2.* Projection of the stress vector onto the deviatoric plane and difference of the yield stress under tensile and shear loading condition.

In pure tensile loading condition, the yield criterion can be defined by  $\sqrt{3J_2} = \sigma_{yt}$ , where  $J_2$  is the second invariant of the deviatoric stress tensor,  $\mathbf{S}$ , and  $\sigma_{yt}$  defines the yield stress in a tensile condition. However, under pure shear loading condition, the yield criterion is written as  $\sqrt{J_2} = \sigma_{ys}$ , where now,  $\sigma_{ys}$  defines the yield stress in shear condition. Based on this behaviour, it can be defined the difference between tensile and shear yield stress,  $\Delta q$ , by:

$$\Delta q = \sigma_{yt} - \sigma_{ys} = (\sqrt{3} - 1)\sqrt{J_2} \quad (8)$$

## 2.2 Lode angle function

The behaviour of the Lode angle, according to the loading condition applied, can be described by *Table 1*.

*Table 1.* Behavior of some elastoplastic parameters.

Load	$\eta$	$\xi$	$\theta$	$\bar{\theta}$
tensile	$1/3$	1	0	1
shear	0	0	$\pi/6$	0
compression	$-1/3$	-1	$\pi/3$	-1

Based on the behaviour of the normalized third invariant or on the Lode angle parameter, a function can be defined, which establishes the influence of the loading condition on the yield criterion of the material. The function can be called as a Lode angle function and is mathematically written as:

$$K_0 = 1 - \xi^2 \quad (9)$$

where  $K_0$  represents the Lode angle function and when it is equals to zero, a predominant tensile or compression loading condition is presented. However, when the function is equal to a unit, a predominant shear loading condition is being applied. Finally, when the function behaves between zero and a unit, a combined loading condition is presented.

## 2.3 Defining the new yield function

In order to define a yield criterion that contemplate the mechanical behaviour in both shear and tensile conditions, the following function is written:

$$\phi = q + \eta_0(\sqrt{3} - 1)(1 - \xi^2)q - \sigma_{yt} \quad (10)$$

where  $\phi$  represents the new yield criterion and the parameter  $\eta_0$  is introduced in order to control the convexity of the function. In this work, it is proposed a non-linear isotropic hardening rule to model the behaviour of the material, as following:

$$\sigma_{yt} = \sigma_{y0} + H^I \bar{\epsilon}^p \quad (11)$$

where  $\sigma_{y0}$  is the initial yield stress of the material under tensile load,  $H^I$  represents the isotropic hardening modulus that is a function of the equivalent plastic strain and  $\bar{\epsilon}^p$  is the equivalent plastic strain that represents the isotropic hardening variable. The isotropic hardening modulus, regarding a non-linear behaviour, is a function of the equivalent plastic strain. The yield function defined in the *Equation* (10) can be plotted and compared to classical yield functions as von Mises and Tresca.

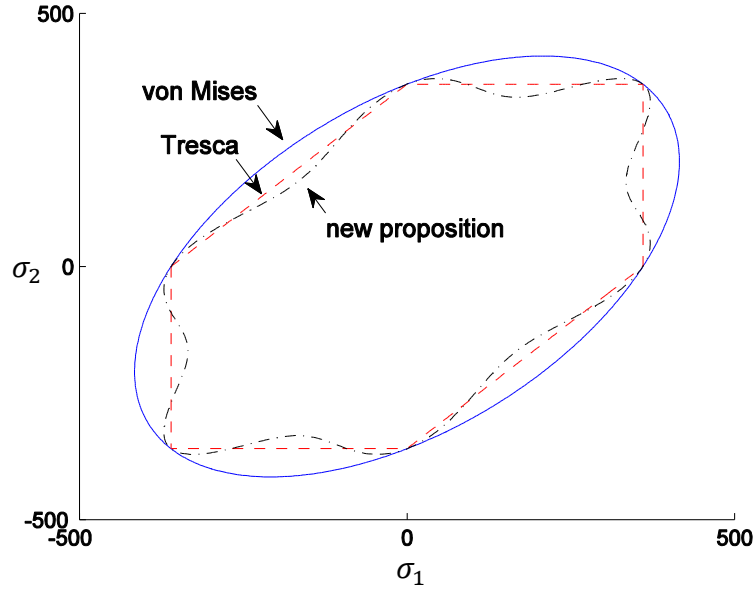


Figure 3. Behaviour of the new proposition ( $\eta_0 = 1/3$ ) and classical yield functions.

Regarding the additive decomposition of the strain tensor, associative plasticity and isotropic hardening, the following mathematical model can be formulated. The convexity of the constitutive model is guaranteed for values of  $\eta_0$  between zero and  $1/3$ .

*Box 1. Mathematical model for the new proposition.*

i) Additive decomposition of the strain tensor:

$$\boldsymbol{\varepsilon} = \boldsymbol{\varepsilon}^e + \boldsymbol{\varepsilon}^p$$

ii) Elastic Law:

$$\boldsymbol{\sigma} = \mathbb{D}^e : \boldsymbol{\varepsilon}^e$$

iii) Yield function:

$$\phi = q + \eta_0(\sqrt{3} - 1)(1 - \xi^2)q - \sigma_{y0} - H^I \bar{\varepsilon}^p$$

$$q = \sqrt{\frac{3}{2} \mathbf{S} : \mathbf{S}}$$

$$\xi = \frac{27 \det \mathbf{S}}{2 q^3}$$

iv) Plastic flow rule:

$$\dot{\boldsymbol{\varepsilon}}^p = \dot{\gamma} \frac{3}{2q} (a_0 \mathbf{S} - a_1 \mathbf{S}^{-1})$$

$$a_0 = 1 + \eta_0(\sqrt{3} - 1)(1 + 5\xi^2) \quad a_1 = \eta_0(\sqrt{3} - 1) \frac{4(q\xi)^2}{3}$$

and evolution of the equivalent plastic strain  $\bar{\varepsilon}^p$  :

$$\dot{\bar{\varepsilon}}^p = \sqrt{\frac{2}{3} \dot{\boldsymbol{\varepsilon}}^p : \dot{\boldsymbol{\varepsilon}}^p} = \dot{\gamma} \sqrt{a_0^2 + a_1^2 \frac{\mathbf{S}^{-1} : \mathbf{S}^{-1}}{\mathbf{S} : \mathbf{S}} - \frac{6a_0 a_1}{\mathbf{S} : \mathbf{S}}}$$

v) Load/unload condition.

$$\dot{\gamma} \geq 0, \quad \phi \leq 0, \quad \dot{\gamma} \phi = 0$$

### 3 NUMERICAL STRATEGY AND CALIBRATION

Regarding the constitutive formulation, an implicit numerical integration algorithm is proposed and based on the operator split methodology (see Simo *et al*, 1998; De Souza Neto *et al*, 2008). The pseudo-time discretization is implemented following the implicit Euler schema. *Box 2* presents the return mapping algorithm developed.

*Box 2.* Numerical integration algorithm.

i) Elastic trial stage: Given a strain increment,  $\Delta\boldsymbol{\varepsilon}$ .

$$\boldsymbol{\varepsilon}_{n+1}^{e\ trial} = \boldsymbol{\varepsilon}_n^e + \Delta\boldsymbol{\varepsilon} \qquad \boldsymbol{\sigma}_{n+1}^{trial} = \mathbb{D}^e : \boldsymbol{\varepsilon}_{n+1}^{e\ trial}$$

$$\Delta\gamma = 0 \qquad \bar{\boldsymbol{\varepsilon}}_{n+1}^{p\ trial} = \bar{\boldsymbol{\varepsilon}}_n^p$$

$$q^{trial} = \sqrt{\frac{3}{2} \mathbf{S}_{n+1}^{trial} : \mathbf{S}_{n+1}^{trial}} \qquad \xi^{trial} = \frac{27 \det \mathbf{S}_{n+1}}{2 q^{trial^3}}$$

ii) Plastic admissibility:

$$\phi^{trial} = q^{trial} + \eta_0(\sqrt{3} - 1)(1 - \xi^{trial^2})q^{trial} - \sigma_{y0} - H^l \bar{\boldsymbol{\varepsilon}}_n^p$$

If  $\phi^{trial} \leq 0$ , then (elastic step):  $(*)_{n+1} = (*_{n+1})^{trial}$ ;

Else (plastic step): Plastic corrector algorithm:

iii) Returning mapping: solve a system of non-linear equations (Newton-Raphson), regarding:  $\boldsymbol{\sigma}_{n+1}$ ,  $\bar{\boldsymbol{\varepsilon}}_{n+1}^p$  e  $\Delta\gamma$ .

$$\left\{ \begin{array}{l} \boldsymbol{\sigma}_{n+1} = \boldsymbol{\sigma}_{n+1}^{trial} - \frac{3G\Delta\gamma}{q_{n+1}} (a_{0\ n+1} \mathbf{S}_{n+1} - a_{1\ n+1} \mathbf{S}_{n+1}^{-1}) \\ \bar{\boldsymbol{\varepsilon}}_{n+1}^p = \bar{\boldsymbol{\varepsilon}}_n^p + \Delta\gamma a_{2\ n+1} \\ \phi = q_{n+1} + \eta_0(\sqrt{3} - 1)(1 - \xi_{n+1}^2)q_{n+1} - \sigma_{y0} - H^l \bar{\boldsymbol{\varepsilon}}_{n+1}^p = 0 \end{array} \right.$$

where:

$$a_{0\ n+1} = 1 + \eta_0(\sqrt{3} - 1)(1 + 5\xi_{n+1}^2)$$

$$a_{1\ n+1} = \eta_0(\sqrt{3} - 1) \frac{4(q_{n+1}\xi_{n+1})^2}{3}$$

$$a_{2\ n+1} = \sqrt{a_{0\ n+1}^2 + a_{1\ n+1}^2 \frac{\mathbf{S}_{n+1}^{-1} : \mathbf{S}_{n+1}^{-1}}{\mathbf{S}_{n+1} : \mathbf{S}_{n+1}} - \frac{6a_{0\ n+1}a_{1\ n+1}}{\mathbf{S}_{n+1} : \mathbf{S}_{n+1}}}$$

iv) Update other state variable:

v) End.

The non-linear equations system is solved by Newton-Raphson method. *Box 3* describes the numerical steps required.

Box 3. Return mapping algorithm (Newton-Raphson).

i) Given the trial state as initial parameters:

$$\boldsymbol{\sigma}_{n+1}^{(0)} = \boldsymbol{\sigma}_{n+1}^{trial} \quad \Delta\gamma^{(0)} = 0 \quad \bar{\varepsilon}_{n+1}^p(0) = \bar{\varepsilon}_n^p$$

ii) Solve the system of equations for:  $\boldsymbol{\sigma}_{n+1}$ ,  $\bar{\varepsilon}_{n+1}^p$  e  $\Delta\gamma$ .

$$\begin{bmatrix} \frac{\partial R_{\boldsymbol{\sigma}_{n+1}}}{\partial \boldsymbol{\sigma}_{n+1}} & \frac{\partial R_{\boldsymbol{\sigma}_{n+1}}}{\partial \bar{\varepsilon}_{n+1}^p} & \frac{\partial R_{\boldsymbol{\sigma}_{n+1}}}{\partial \Delta\gamma} \\ \frac{\partial R_{\bar{\varepsilon}_{n+1}^p}}{\partial \boldsymbol{\sigma}_{n+1}} & \frac{\partial R_{\bar{\varepsilon}_{n+1}^p}}{\partial \bar{\varepsilon}_{n+1}^p} & \frac{\partial R_{\bar{\varepsilon}_{n+1}^p}}{\partial \Delta\gamma} \\ \frac{\partial R_{\Delta\gamma}}{\partial \boldsymbol{\sigma}_{n+1}} & \frac{\partial R_{\Delta\gamma}}{\partial \bar{\varepsilon}_{n+1}^p} & \frac{\partial R_{\Delta\gamma}}{\partial \Delta\gamma} \end{bmatrix}^k \cdot \begin{bmatrix} \delta \boldsymbol{\sigma}_{n+1} \\ \delta \bar{\varepsilon}_{n+1}^p \\ \delta \Delta\gamma \end{bmatrix}^{k+1} = - \begin{bmatrix} R_{\boldsymbol{\sigma}_{n+1}} \\ R_{\bar{\varepsilon}_{n+1}^p} \\ R_{\Delta\gamma} \end{bmatrix}^k$$

iii) Determine:

$$\boldsymbol{\sigma}_{n+1}^{(k+1)} = \boldsymbol{\sigma}_{n+1}^{(k)} + \delta \boldsymbol{\sigma}_{n+1}^{(k+1)} \quad \Delta\gamma^{(k+1)} = \Delta\gamma^{(k)} + \delta \Delta\gamma^{(k+1)}$$

$$\bar{\varepsilon}_{n+1}^p(k+1) = \bar{\varepsilon}_{n+1}^p(k) + \delta \bar{\varepsilon}_{n+1}^p(k+1)$$

iv) Convergence:

$$\phi^{(k+1)} = q^{(k+1)} + \eta_0(\sqrt{3} - 1) \left(1 - \xi^{(k+1)^2}\right) q^{(k+1)} - \sigma_{y0} - H^I \bar{\varepsilon}_{n+1}^p(k+1)$$

$$error = \frac{\phi^{(k+1)}}{\left[\sigma_{y0} + H^I \bar{\varepsilon}_{n+1}^p(k+1)\right]} \leq tolerance$$

v) End.

According to the numerical implementation, the hardening curve is determined by a calibration procedure. The strategy starts with experimental results for a smooth bar specimen under pure tensile loading condition. A aluminum alloy 2024-T351 is also used, presenting the following material properties:  $E = 72400 \text{ MPa}$ ,  $\nu = 0.33$  and  $\sigma_{y0} = 352 \text{ MPa}$ . In order to determine the hardening curve, the gradient method is taken by a univariable search squema. *Figure 4* shows the results after the application of the calibration strategy.

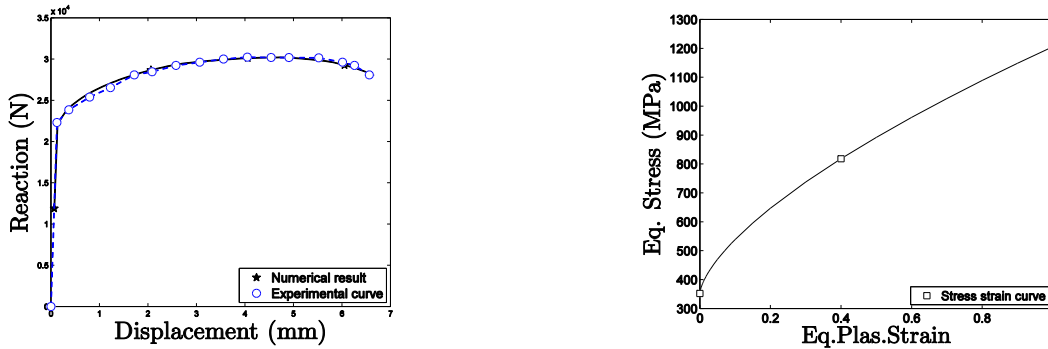


Figure 4. Reaction curve and hardening curve for the aluminum alloy.

## 4 NUMERICAL RESULTS

Some preliminary tests were performed in order to demonstrate the robustness of the constitutive formulation. The aluminum alloy 2024-T351 was taken as well as specimens under different loading conditions. *Figure 5* displays numerical and experimental results obtained regarding reaction curves for: (a) flat grooved plate under tensile, (b) butterfly specimen under shear and (c) shear specimen. In both cases, the proposed model has demonstrated a good agreement with the experimental data. In the first case (a), the correction in the reaction curve was around 20% when the third invariant effect is introduced. In cases (b) and (c), the correction was by around 30%.

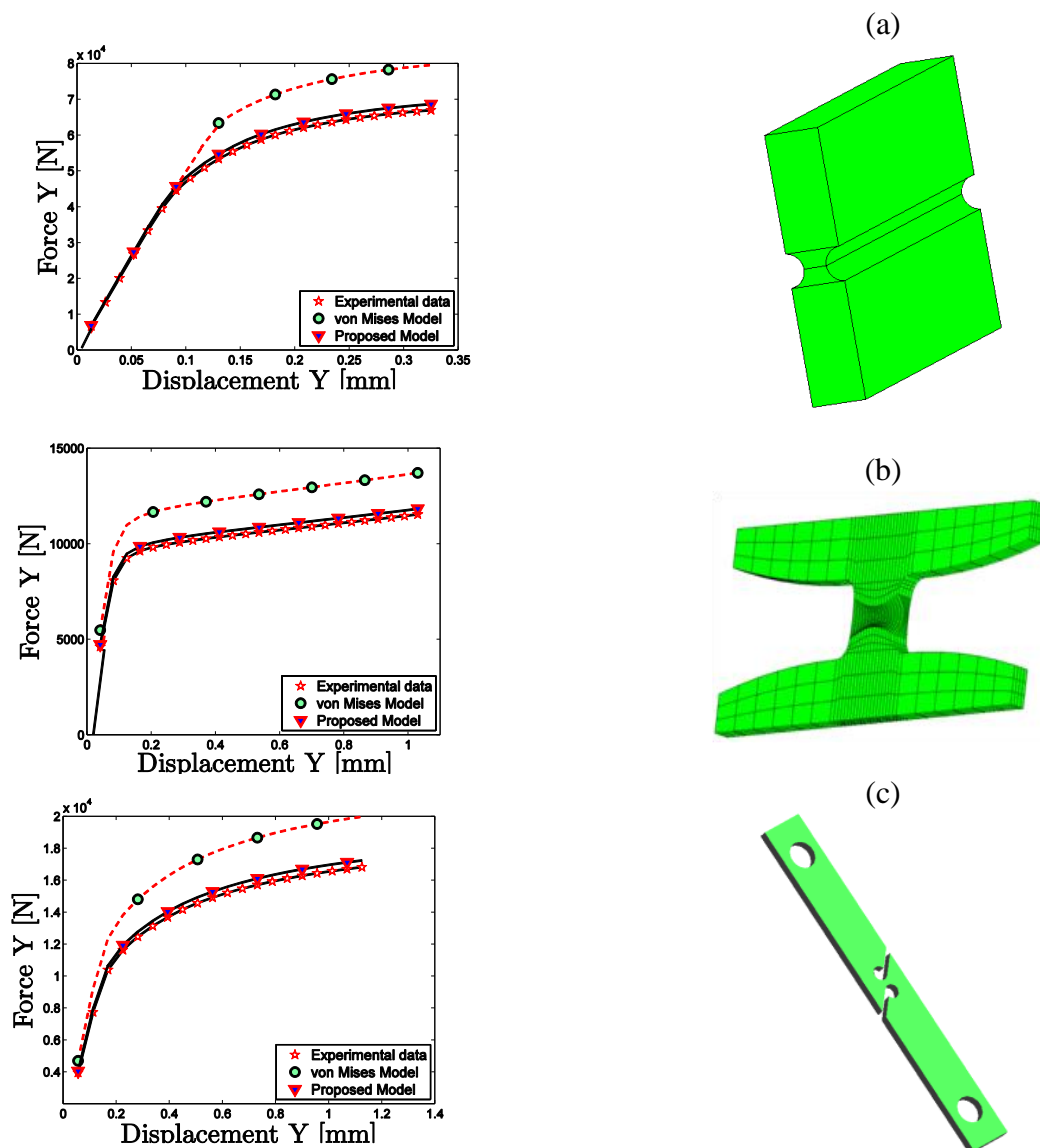


Figure 5. Reaction curves for specimens under different loading conditions.

## 5 CONCLUSION

In this contribution, the influence of the third invariant was studied through a constitutive model proposed here. A flat grooved plate specimen and two shear specimens were used as well as a strongly dependent on the third invariant material, as the aluminium alloy 2024-T351. According to the numerical results presented, it can be observed the importance of the third invariant on the plastic flow rule for ductile materials. The correction in the reaction *versus* displacement curves, when the third invariant effect is active, is evident. In the critical presented case, the analysed curve regarding the model without the effect of third invariant, presents an error of 30%; when compared to the experimental data.

## REFERENCES

- [1] Bai, Y., Wierzbicki, T. (2007). A new model of metal plasticity and fracture with pressure and Lode dependence, *International Journal of Plasticity*, 24:1071-1096.
- [2] Bai, Y. (2008). Effect of Loading History on Necking and Fracture. Ph.D Thesis, Massachusetts Institute of Technology.
- [3] Bao, Y., Wierzbicki, T. (2004). On fracture locus in the equivalent strain and stress triaxiality space. *International Journal of Mechanical Sciences*. 46 (81):81-98.
- [4] Bardet, J. P. (1990). Lode Dependence for Isotropic Pressure-Sensitive Elastoplastic materials. *Jornal of Applied Mechanics*, 57:498-506.
- [5] Barsoum, I., Faleskog, J. (2007a). Rupture in combined tension and shear: experiments. *International Journal of Solids and Structures*, 44:1768–1786.
- [6] Barsoum, I., Faleskog, J. (2007b). Rupture in combined tension and shear: micromechanics. *International Journal of Solids and Structures*, 44:5481–5498.
- [7] Brünig, M., Chyra, O., Albrecht, D., Driemeier, L., Alves, M. (2008). A ductile damage criterion at various stress triaxialities, *International Journal of Plasticity*, 24: 1731–1755.
- [8] Brünig, M., Berger, S., Obrecht, H. (2000). Numerical simulation of the localization behavior of hydrostatic-stress-sensitive metals. *International Journal of Mechanical Sciences*, 42:2147-2166.
- [9] Brünig, M., (1999). Numerical simulation of the large elastic-plastic deformation behavior of hydrostatic stress-sensitive solids. *International Journal of Plasticity* 15, 1237-1264.
- [10] De Souza Neto, E.A., Peri'c, Owen, D.R.J. (2008). *Computational methods for plasticity: theory and applications*. John Wiley & Sons Ltd.
- [11] Driemeier, L., Brünig, M., Micheli, G., Alves, M., (2010), Experiments on stress-triaxiality dependence of material behavior of aluminum alloys, *Mechanics of Materials*, vol.42, 2:207-217.
- [12] Gao, X., Zhang, T., Zhou, J., Graham, S.M., Hayden, M., Roe, C. (2011), On stress-state dependent plasticity modeling: Significance of the hydrostatic stress, the third invariant of stress deviator and the non-associated flow rule, *International Journal of Plasticity*, vol. 27, 2:217-231.

- [13] Mirone, G., Corallo, D., (2010), A local viewpoint for evaluating the influence of stress triaxiality and Lode angle on ductile failure and hardening, *International Journal of Plasticity*, vol. 26, 3:348-371.
- [14] Nahshon, K., Hutchinson, J. (2008). Modification of the Gurson model for shear failure. *European Journal of Mechanics A/Solids*, 27:1–17.
- [15] Richmond, O. and Spitzig, W. A., (1980). Pressure dependence and dilatancy of plastic flow. In *Theoretical and Applied Mechanics, Proceedings of the 15th International Congress of Theoretical and Applied Mechanics.*, pages 377–386, Toronto, Ont, Can, 1980. North-Holland Publ Co, Amsterdam, Neth.
- [16] Simo, J.C., & Hughes, T.J.R. (1998). *Computational Inelasticity*. New York: Springer-Verlag.
- [17] Tvergaard, V. (2008). Shear deformation of voids with contact modeled by internal pressure. *International Journal of Mechanical Sciences*, 50:1459–1465.
- [18] Wilson, C., D., (2002), A critical re-examination of classical metal plasticity. *Journal of Applied Mechanics, Transactions ASME*, 69(1):63–68, ISSN 0021-8936.
- [19] Xue, L. (2008). Constitutive modeling of void shearing effect in ductile fracture of porous materials. *Engineering Fracture Mechanics*, 75: 3343–3366.
- [20] Zadpoor, A.A., Sinke, J., Benedictus, R. (2009). Formability prediction of high strength aluminum sheets, *International Journal of Plasticity*, 25:2269–2297.